Effect of Deposited Bismuth on the Potential of Maximum Entropy of Pt(111) Single-Crystal Electrodes

V. Climent,*,† N. Garcia-Araez,† R. G. Compton,‡ and J. M. Feliu†

Instituto de Electroquímica, Universidad de Alicante, ap. 99, E−03080, Alicante, Spain, and Physical and Theoretical Chemistry Laboratory, Oxford University, South Parks Road, Oxford OX1 3QZ, United Kingdom

Received: March 30, 2006; In Final Form: August 17, 2006

The effect of bismuth adsorption on the entropy of formation of the double layer on Pt(111) electrodes has been studied with the laser-induced temperature jump method. The coulostatic response to the temperature change induced by pulsed laser illumination allows the estimation of the sign and magnitude of the thermal coefficient of the potential drop at the interphase. This is related to the entropy of formation of the double layer, and the particular potential where this thermal coefficient becomes zero can be identified with the potential of maximum entropy of double-layer formation (pme). The effect of bismuth adsorption on the pme depends on the adatom coverage. At high coverages, a marked decrease of the pme is observed. This trend follows the change of the potential of zero charge expected from work function measurements, and it is likely due to the change in the orientation of solvent molecules induced by surface dipoles originated between the adatom and the substrate. At low coverage, the pme increases with the bismuth coverage. The disruption of the water structure due to the presence of the bismuth adatoms is tentatively proposed as the most likely explanation for this behavior.

1. Introduction

The modification of the surface composition of platinum single-crystal electrodes by deposition of foreign metals adatoms is a subject extensively investigated. Both s^2p^n and transition metals have been deposited in order to alter the electrocatalytic properties of platinum electrodes. The behavior of such bimetallic surfaces has been tested for model fuel cell reactions in numerous studies. These investigations include reactions such as formic acid oxidation,[1−14] oxygen reduction,[15] and hydrogen evolution.[16−18]

Among the different surface modifiers, metals from groups 15 and 16 of the periodic table exhibit the ability of being irreversibly deposited on platinum surfaces.[19−25] One of the systems more extensively studied is bismuth onto Pt(111) electrodes.[18,19,26−35] This combination exhibits interesting electrocatalytic properties for the oxidation of small molecules, like CO[36] and formic acid.[1,6,13,37−39] The modified electrodes exhibit a couple of redox processes, whose charge is related with the amount of deposited bismuth. By comparing the charge of this redox process with the blockage of hydrogen adsorption, it is possible to calculate the ratio between the number of electrons transferred in this process and the number of blocked sites on the Pt substrate. This number depends on the nature of the adatom, being two electrons for bismuth on Pt(111).[19] In consequence, the amount of deposited adatom can be easily characterized by measuring the charge under this process. Moreover, the peak potential shifts 60 mV per pH unit. On the basis of these observations, it was postulated that this process corresponds to the oxidation of the adsorbed adatoms, either by OH adsorption or by oxide formation, without desorption to the solution.[19] Similar observations have been reported for other s^2p^n adatoms,[20−25] and in some cases, the changes occurring during the oxidation of the modified surface have been monitored by non-electrochemical techniques, such as STM[40,41] and XPS.[42,43]

We have shown recently that laser illumination can be used to induce a jump on the temperature of the surface of single-crystal electrodes.[44−46] This technique was previously used with mercury electrodes[47] and with polycrystalline platinum.[48] The response of the electrode potential to the change of the temperature gives a measure of the temperature coefficient of the potential drop at the double layer. This coefficient is related with the entropy of formation of the double layer: the potential where this coefficient becomes zero corresponds to the potential of maximum entropy (pme) of double-layer formation.[47,49]

We have applied this method to the study of Au(111) single-crystal electrodes.[44] The results obtained in the absence of specific adsorption reproduce well previous studies using conventional electrochemical techniques.[50] When the electrochemical behavior is complicated with specific adsorption, the time of the response to the temperature change becomes longer, and it is necessary to take into account the kinetics of the relaxation.

One of the advantages of this technique is the possibility of decoupling the charge transfer process associated with adsorption phenomena from the purely double-layer response, by making the temperature jump sufficiently fast. Besides, the rate of the adsorption process can be modified by changing the concentration of species in the solution. This strategy was applied to Pt(111) single-crystal electrodes:[45] in acidic solution, the rate of hydrogen adsorption is fast enough to have an effect on the response to a change of the temperature in the submicrosecond time scale; however, when the proton concentration is lowered, the hydrogen adsorption reaction is slowed down, and

* Corresponding author: victor.climent@ua.es.
† Universidad de Alicante.
‡ Oxford University.

10.1021/jp061982i CCC: $33.50
Published on Web 09/29/2006

it does not take place on the same time scale. Then, the measured potential change represents mainly the response of the double layer, thus allowing the determination of the pme of double-layer formation for this electrode.

According to classical models, the pme of double-layer formation can be approximately identified with the potential where the turnover of water molecules takes place,[49] which is, in addition, related to the potential of zero charge (pzc) of the surface. Then, if the surface is negatively charged, we can expect the water molecules to be polarized with the positive end closer to the metal, while the opposite is true when the surface is positively charged. The picture is complicated by the existence of a chemical interaction between the water molecules and the metal surface that orient the water molecules even in the absence of any electric field. This natural orientation is with the oxygen interacting with the metal surface in the case of gold electrodes, as reflected in the fact that the pme is located slightly negative to the pzc.

In this paper, we investigate the effect of bismuth adsorption on the pme of double-layer formation. In ultrahigh vacuum, bismuth deposition causes a marked decrease of the work function of a Pt (111) surface.[51] Given the parallelism between the work function and the pzc,[52] a decrease of this parameter is also expected in the electrochemical environment. This decrease of the pzc plays an important role in the understanding of the electrocatalytic effect of the bimetallic surface. As we show in this paper, the deposition of bismuth onto a Pt(111) electrode surface also causes a decrease of the pme when the coverage is high enough. However, at low and intermediate coverages, the picture is more complicated.

2. Experimental Section

2.1. Electrode Preparation. The Pt(111) electrode was prepared from a small platinum bead (2 mm), oriented, cut, and polished to obtain the desired orientation, following Clavilier's procedure.[53] Prior to each experiment, the electrode was annealed in a Bunsen flame (propane−air), cooled in a flow of argon (N-50, Air Liquide), and protected with a drop of ultrapure water, deaerated with argon.

After recording a voltammogram to ensure the quality of the surface and the cleanliness of the solution, the electrode was immersed in a 0.1 M $HClO_4$ solution saturated with Bi_2O_3 (for lower coverages, more dilute solutions were prepared by diluting the saturated solution 10 or 100 times in 0.1 M $HClO_4$) for a time between 5 and 90 s. Then, the electrode was rinsed with ultrapure water and transferred to the electrochemical cell, where a new voltammogram was recorded to characterize the bismuth coverage achieved during the adsorption step.

2.2. Laser-Induced Temperature Jump Measurement. The experimental protocol has been described elsewhere.[44] Briefly, after recording a voltammogram to ensure the surface order and cleanliness of the solution, the electrode is polarized at a given potential. Around 200 μs before firing the laser, the potentiostat is disconnected, and the open circuit potential of the working electrode is measured while the laser is fired at the surface, producing the rise of the temperature. The experiment was repeated at a frequency of 10 Hz, which allows the relaxation of the temperature to its room value between consecutive pulses. The potentiostat is reconnected between successive laser pulses, ensuring that the potential is kept at the desired value. Two different methods were used to follow the time evolution of the potential of the working electrode. In the first method, the working electrode is connected to ground, while the potential of the reference electrode is measured versus ground with a fast amplifier. To keep the circuit open, the counter electrode is disconnected just before firing the laser. In the second method, a fourth platinum electrode is immersed in the cell and polarized exactly at the same potential as the working electrode. Just before firing the laser, both electrodes are disconnected from the potentiostat, and the potential difference between them is measured with a differential amplifier. The potential difference is due to the laser heating of just the working electrode. The advantage of this second method is that other potential fluctuations not due to the laser illumination (noise) are expected to cancel when the potential of both electrodes is subtracted. In fact, a better signal-to-noise ratio is obtained with the second method, although essentially the same results are obtained with both procedures. In any case, 128 or 256 potential transients were averaged at each potential using a TDS 3054B Tektronix oscilloscope. After recording the laser transients at different potentials, a new voltammogram was recorded and compared with the initial one, to test the stability of the surface in the whole experiment. Only those experiments in which the charge of the final voltammogram was no more than 5% lower than the initial one were kept as meaningful.

The light source employed was a Brilliant Q-switched Nd:YAG laser (Quantel) operating in frequency-doubled mode at a wavelength of 532 nm and pulse duration of 5 ns. The beam diameter obtained directly at the laser output is ca. 6 mm, and this was reduced to ca. 4 mm by passing it through a conventional arrangement of lenses. Laser energy of ca. 1 mJ per pulse, i.e., 8 mJ cm^{-2}, was used in all the experiments, well below the damage threshold of the electrode surface.

2.3. Electrochemical Cell, Instrumentation, and Solutions. All experiments were performed in a conventional three-electrode configuration. A coiled platinum wire was used as a counter electrode and a hydrogen-charged Pd wire was used as a reference electrode, which equals +50 mV vs RHE (reversible hydrogen electrode). All potentials in this work are quoted against the RHE scale in order to facilitate the comparison with other studies, except for those in Figure 9. The potential of the reference was measured at the end of each experiment against a saturated calomel electrode, and this value was used to convert potentials to the standard hydrogen electrode (SHE) scale in Figure 9. Cyclic voltammograms were recorded using a computer-controlled μ-Autolab potentiostat (Eco-Chemie, Utrecht, The Netherlands) under the current integration mode.

Solutions were prepared from concentrated perchloric acid (Merck, suprapur) and $KClO_4$ (Merck, p.a.) diluted in ultrapure water (18.2 MΩ cm) obtained from a Elgastat water purification system. The $KClO_4$ was purified by recrystallization, and the $HClO_4$ was used as received. Bismuth solutions were prepared from Bi_2O_3 (Merck, extra pure). The electrolytes were purged with argon (N50, Air Liquide), and the solution was kept under an argon blanket throughout the duration of the experiment.

3. Results and Preliminary Data Interpretation

Figure 1 shows cyclic voltammograms obtained with the Pt(111) single-crystal electrode covered with different amounts of bismuth in 0.1 M $HClO_4$ solution. Different coverages were achieved by selecting different adsorption times and/or different bismuth(III) concentrations. The more salient features observed in those voltammograms are similar to what has been previously reported:[19] as the bismuth coverage increases, the hydrogen adsorption decreases, and a new voltammetric peak appears at ca. 0.67 V. This peak has been attributed to the oxidation of

surface adatoms[19]

$$Pt(111)-Bi + 2H_2O \rightarrow Pt(111)-Bi(OH)_2 + 2H^+ + 2e$$

or

$$Pt(111)-Bi + H_2O \rightarrow Pt(111)-BiO + 2H^+ + 2e$$

According to this interpretation, the charge under this peak can be used to characterize the bismuth coverage. Unlike the experiments performed in sulfuric acid,[19] the Bi-related peak is overlapped with the adsorption states between 0.55 and 0.85 V, characteristic of the clean Pt(111) electrode in perchloric acid solution, usually assigned to OH adsorption.

Alternatively, the amount of bismuth on the surface can be quantified by measuring the blockage of the hydrogen adsorption reaction. It has been proposed that each adsorbed bismuth blocks three Pt(111) sites.[19,27] Then

$$q_H^\theta = q_H^{\theta=0}(1 - 3\theta) \quad (1)$$

where q_H^θ and $q_H^{\theta=0}$ represent the hydrogen adsorption charge in the presence and in the absence of bismuth, respectively. Therefore, bismuth coverage could be estimated using eq 1. Moreover, if we accept that the degree of blockage for OH adsorption depends on the bismuth coverage similarly to eq 1

$$q_{OH}^\theta = q_{OH}^{\theta=0}(1 - 3\theta) \quad (2)$$

It is possible to use eq 2 to correct the charge integrated between 0.55 and 0.75 V in order to obtain the charge corresponding only to the surface redox process associated with bismuth. The latter should be proportional to the bismuth coverage according to

$$q_{Bi}^\theta = \frac{\theta}{\theta_{max}} q_{Bi}^{\theta_{max}} \quad (3)$$

from eqs 1 and 3, it is possible to eliminate θ

$$q_{Bi}^\theta = q_{Bi}^{\theta_{max}} - \frac{q_{Bi}^{\theta_{max}}}{q_H^{\theta=0}} q_H^\theta \quad (4)$$

where θ_{max} has been taken as 0.33 as suggested by eq 1. This maximum coverage is in agreement with identified structures characterized by ultrahigh vacuum (UHV) measurements on adlayers prepared both in UHV[51] and electrochemical environments.[28] Accordingly, a straight line is expected when plotting q_{Bi}^θ vs q_H^θ as already shown in reference for results obtained in sulfuric acid.[27] The intercepts of this line with the axes should be (0, $q_{Bi}^{\theta_{max}}$) and ($q_H^{\theta=0}$, 0). Open circles in Figure 2 show the result of such a plot. They are reasonably aligned in a straight line. The intercept when $q_{Bi}^\theta = 0$ is ca. 160 μC cm^{-2}, which is the well-accepted value for $q_H^{\theta=0}$ for Pt(111) in 0.1 M $HClO_4$. On the other hand, the extrapolated value for $q_{Bi}^{\theta_{max}}$ is ca. 160 μC cm^{-2}, in agreement with the values published previously.[19] However, there are points with a full blockage for hydrogen adsorption and a bismuth charge higher than 160 μC cm^{-2}. This fact is explained by the further adsorption of bismuth in a more compact adlayer.[27]

Experiments were repeated in a 0.1 M $KClO_4$ + 1 mM $HClO_4$ solution. The use of a working solution with a higher pH has a double purpose. First, it decreases the thermodiffusion potential that arises because of the temperature difference between the heated solution near the working electrode and the cold solution near the reference electrode.[44] Although this contribution is small compared with the response of the double layer, it is not negligible in solutions of low pH, due to the abnormally high entropy of transport of the protons.[54] On the other hand, it has been shown that hydrogen adsorption complicates the interpretation of the laser-induced potential transients in 0.1 M $HClO_4$ solution[45] (see below). The decrease of the proton concentration decreases the rate of hydrogen adsorption, almost eliminating this problem at pH = 3. Under these conditions, it is possible to decouple the response of the double layer from the hydrogen adsorption process. Figure 3 shows cyclic voltammograms in the solution of pH = 3, corresponding to a Pt(111) electrode modified with different bismuth coverages in the submonolayer range. The main features in the voltammogram are similar to those of Figure 1, obtained in the lower pH solution. The only remarkable difference between the voltammograms obtained at

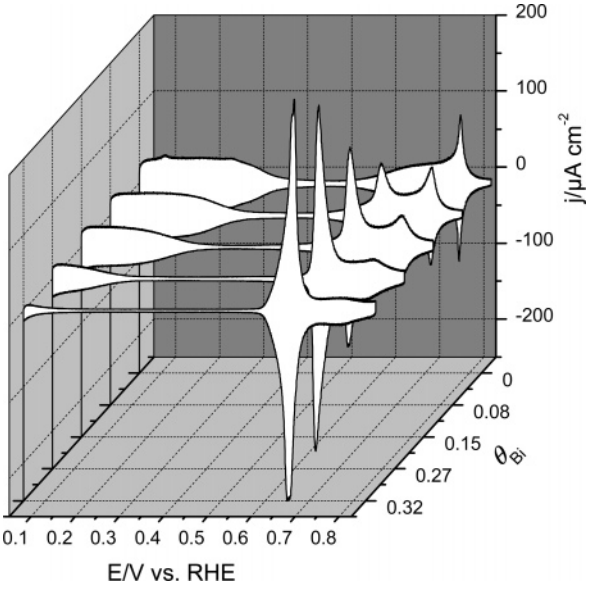

Figure 1. Cyclic voltammetric profiles corresponding to a Bi-modified Pt(111) electrode surface with different bismuth coverages in 0.1 M $HClO_4$ solution. Sweep rate: 50 mV s^{-1}.

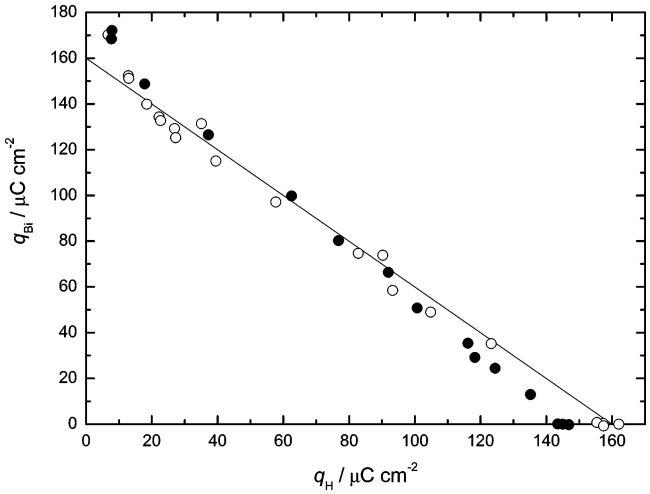

Figure 2. Plot of the charge integrated under the bismuth redox process as a function of the remaining hydrogen charge for a bismuth-modified Pt(111) electrode in (a) 0.1 $HClO_4$ (open circles) and (b) 0.1 M $KClO_4$ + 1 mM $HClO_4$ (closed circles).

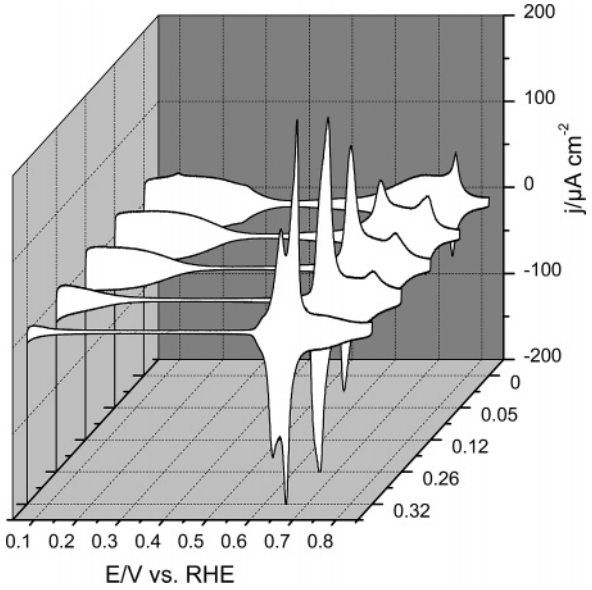

Figure 3. Cyclic voltammetric profiles corresponding to a Bi-modified Pt(111) electrode surface with different bismuth coverages in 0.1 M $KClO_4$ + 1 mM M $HClO_4$ solution. Sweep rate: 50 mV s^{-1}.

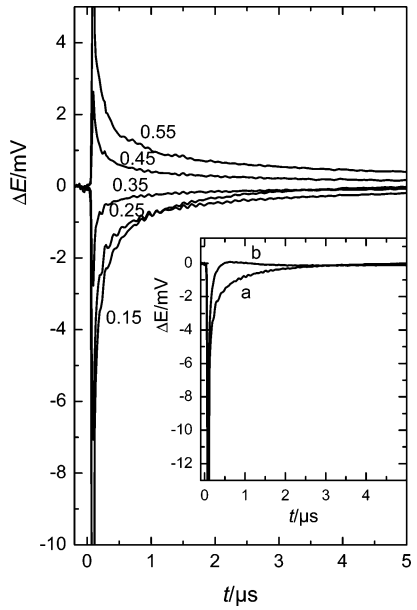

Figure 4. Laser-induced coulostatic potential transients corresponding to a Bi−Pt(111) electrode with $\theta = 0.23$ in 0.1 M $HClO_4$, obtained at different potentials, as labeled in the figure. Inset: comparison of the potential transients obtained at 0.15 V with (a) Bi ($\theta = 0.23$) and (b) Bi-free Pt(111) electrode.

both pHs is observed at $\theta_{Bi} > 0.28$, where the peak corresponding to the redox process on the bismuth splits into two peaks. This splitting is not observed at pH = 1 unless the bismuth coverage exceeds 0.33.[27] In this latter case, the new peaks observed at high coverage were attributed to the formation of more compact adlayers,[27] as those described in UHV. If the same explanation holds at pH = 3, we could tentatively propose that the (partial) formation of a more compact adlayer is easier at higher pH. However, there is no other experimental evidence for this fact.

As discussed above, a plot of the charge integrated under the bismuth peak, as a function of the remaining hydrogen charge, should give a straight line, according to eq 4. Closed circles in Figure 2 correspond to the charges measured at pH = 3. For low bismuth coverages, hydrogen charges are slightly smaller than those predicted by the theoretical line, leading to an intercept corresponding to zero bismuth coverage equal to ca. 145 μC cm^{-2}. This decrease of the maximum hydrogen coverage when the pH is increased, while maintaining the same integration domain, is in accordance with the values previously published.[55] On the other hand, at high bismuth coverage, the values deviate slightly above the theoretical line, resulting in an intercept at $q_H = 0$ equal to ca. 170 μC cm^{-2}. As discussed above, higher bismuth charges can be due to the formation of small patches with a compressed structure.[27] However, it cannot be ruled out that some of the deviation is due to OH adsorption not fully accounted for by eq 2.

Figure 4 shows potential transients induced by laser illumination obtained in 0.1 M $HClO_4$ at different electrode potentials with a Pt(111) electrode covered by bismuth at a coverage 0.23. On the other hand, the inset in Figure 4 shows the comparison between the potential transient measured at 0.15 V with and without bismuth on the surface of the electrode.

To understand the shape of the laser-induced potential transient, the effect of the laser illumination on the surface of the electrode must be recalled. The main assumption is that the only effect caused by the laser illumination is the increase of the interfacial temperature. Although the exact temperature of the interface cannot be measured, due to the short time scale of the perturbation, it can be calculated through a very simple model, considering that the fraction of the energy of the laser pulse that is not reflected on the surface is converted immediately into heat at the surface of the electrode.[56] The temperature change can be calculated by solving the following partial differential equation

$$\frac{\partial^2 \Delta T}{\partial x^2} = \frac{1}{\alpha_i}\frac{\partial \Delta T}{\partial t} \tag{5}$$

subject to the following boundary conditions

$$-\kappa_1 \frac{\partial \Delta T}{\partial x}\Big|_{x=0^-} = -q' \quad \text{heat flux into solution} \tag{6}$$

$$-\kappa \frac{\partial \Delta T}{\partial x}\Big|_{x=0^+} = q - q' \quad \text{heat flux into the metal} \tag{7}$$

$$\Delta T(x, t=0) = 0 \tag{8}$$

$$\lim_{x \to \pm\infty} \Delta T(x,t) = 0 \tag{9}$$

In this model, the surface of the metal is located at $x = 0$, $x < 0$ corresponds to the solution, and $x > 0$ to the metal; q is the flux of heat absorbed at the surface of the electrode, i.e., the part of the radiation that is not reflected

$$q = (1 - R)I \tag{10}$$

where I is the laser intensity (considered spatially uniform) and R is the reflectivity of the surface. q' is the heat flux conducted into the solution, and κ, α and κ_1, α_1 are the thermal conductivity and the thermal diffusivity of the metal and the aqueous solution, respectively ($\alpha = \kappa/\rho c$, where ρ is the density and c is the heat capacity).

By solving eq 5, the following expression is obtained for the temperature change at the interface[47,57]

$$\Delta T(t) = \left[\frac{\kappa}{\sqrt{\alpha}} + \frac{\kappa_1}{\sqrt{\alpha_1}}\right]^{-1} \int_0^t \frac{(1 - R)I(t - t')}{\sqrt{\pi t}}\, dt' \tag{11}$$

If a uniform laser pulse is considered, the following expression results

$$\Delta T = \frac{2(1-R)I}{\sqrt{\pi}}\left[\frac{\kappa}{\sqrt{\alpha}} + \frac{\kappa_1}{\sqrt{\alpha_1}}\right]^{-1}(\sqrt{t} - \sqrt{t-t_0}) \quad t > t_0 \tag{12}$$

where t_0 is the pulse width. Substituting $t = t_0$ in eq 12, the maximum temperature change achieved at the surface of the electrode can be calculated. For $I = 1.6$ MW cm^{-2} and $t_0 = 5$ ns, a maximum $\Delta T = 35$ K is predicted, considering $R = 0.55$.[58] For $t \gg t_0$, the expression above can be simplified to

$$\Delta T = \frac{1}{2}\Delta T_0\sqrt{\frac{t_0}{t}} \tag{13}$$

where ΔT_0 is the maximum temperature change at $t = t_0$. Since all measurements shown in this paper are performed at $t > 100$ ns, much larger than the pulse duration, 5 ns, the previous simplified expression is accurate to reflect the relaxation of the temperature at the interface after the laser pulse. Other refinements, such as considering the true spatial and temporal distribution of the laser intensity or the finite penetration depth of the light in the metal (this is typically around several nanometers[56]), would improve the estimation of the maximum ΔT, but they do not add relevant information for the discussion that follows. Temperature transients calculated with different degrees of approximation were compared in ref 44.

It has been shown that, among the different contributions to the potential change, the main term comes from the response of the double layer. Other contributions are due to the existence of a thermodiffusion potential, between the heated solution at the surface of the electrode and the cold solution near the reference electrode, and the potential difference between the heated and cold parts of the metal.[47] However, these contributions are significantly smaller than the change of the potential drop at the interface induced by the change of the temperature.[47] For an infinitely fast response of the double layer potential to the temperature change, a monotonic decay of the potential is expected, according to

$$\Delta E = \left(\frac{\partial \Delta_S^M \phi}{\partial T}\right)_q \frac{1}{2}\Delta T_0\sqrt{\frac{t_0}{t}} \tag{14}$$

where the term $(\partial\Delta_S^M\phi/\partial T)_q$ represents the temperature coefficient of the double layer. Such monotonic decays were obtained for the Au(111) single-crystal electrode in the absence of specific anion adsorption.[44] However, for the Pt(111) electrode in 0.1 M $HClO_4$, a non-monotonic decay of the potential change is obtained in the region of hydrogen adsorption.[45] This shape is observed in the transient obtained at 0.15 V on the Bi free, unmodified Pt(111) electrode, shown in the inset of Figure 4. This behavior has been interpreted considering the finite rate of the hydrogen adsorption reaction that responds to the temperature change with a relatively slow relaxation time.[45] In agreement with the previous interpretation, this non-monotonic behavior is less notable when the hydrogen adsorption process is partially blocked by the bismuth adatoms. In the absence of kinetic complications, the first important piece of information that can be gained is the sign of the temperature coefficient of the double layer, $(\partial\Delta_S^M\phi/\partial T)_q$. According to Figure 4, this is negative when the experiment is performed at low potential values and changes to positive when the electrode potential is increased above 0.45 V. The laser-induced potential transients remain positive for $E > 0.45$ V, even within the potential range associated with the oxidation of the bismuth adlayer. However, for experiments at potentials located under the bismuth peak, the transients do not follow the temperature change (not shown), evidencing that the bismuth oxidation is slow in this time scale (this point will be discussed later in more detail).

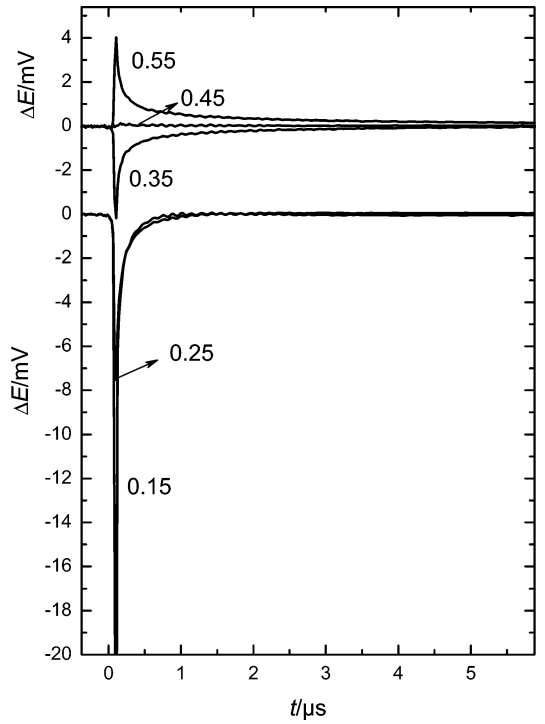

Figure 5. The same as Figure 4, except for a Bi coverage of 0.12. The curves have been separated in two plots for the sake of clarity.

For a lower bismuth coverage, the hydrogen adsorption process is not totally blocked, and it interferes with the change of the potential induced by the laser heating. Figure 5 shows laser-induced potential transients obtained with a bismuth coverage of 0.12. A faster decay of the potential transient is observed at low potential values, resembling that of the bismuth-free Pt(111) electrode surface. Although this shape complicates the interpretation of the potential transient, it is still clear that the transients change sign again around 0.45 V. As for higher bismuth coverage, the transients become more complex at potentials located under the bismuth peak.

As commented before, the experiment was repeated at a higher pH, with the double purpose of decreasing the thermodiffusion potential and the interference due to the hydrogen adsorption process. Figure 6 shows laser-induced potential transients obtained with a Pt(111) electrode covered with a bismuth coverage equal to 0.24 in 0.1 M $KClO_4$ + 1 mM $HClO_4$. The trend is the same as that observed at pH = 1: negative transients at low potential and positive transients at high potentials. The effect of the coverage on the potential transients is shown in Figure 7, at two selected potentials: 0.15 and 0.45 V. At the lower potential range, the transients are negative, remaining nearly constant except for bismuth coverage near saturation ($\theta_{Bi} > 0.3$), when the intensity of the potential perturbation decreases. On the other hand, a significant effect of the bismuth coverage is observed in the transients measured at 0.45 V. In this case, although the potential transient is negative for the unmodified electrode at this pH, it becomes positive after increasing the bismuth coverage. This potential value (0.45 V) is close to the pzt, and this trend reflects the effect of bismuth on this parameter.

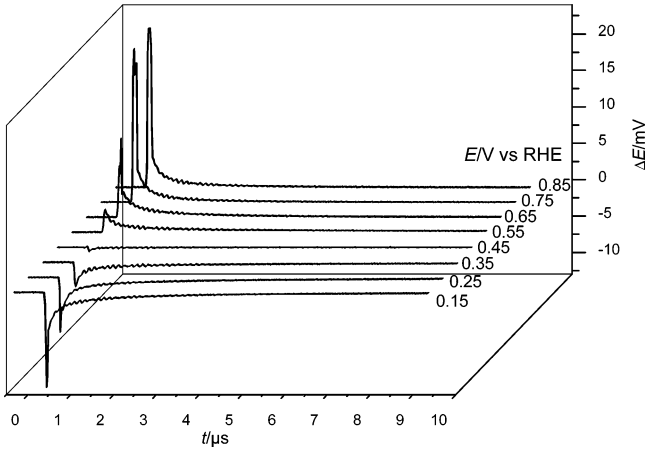

Figure 6. Laser-induced coulostatic potential transients corresponding to a Bi−Pt(111) electrode with $\theta_{Bi} = 0.24$ in 0.1 M $KClO_4$ + 1 mM $HClO_4$, obtained at different potentials, as labeled in the figure.

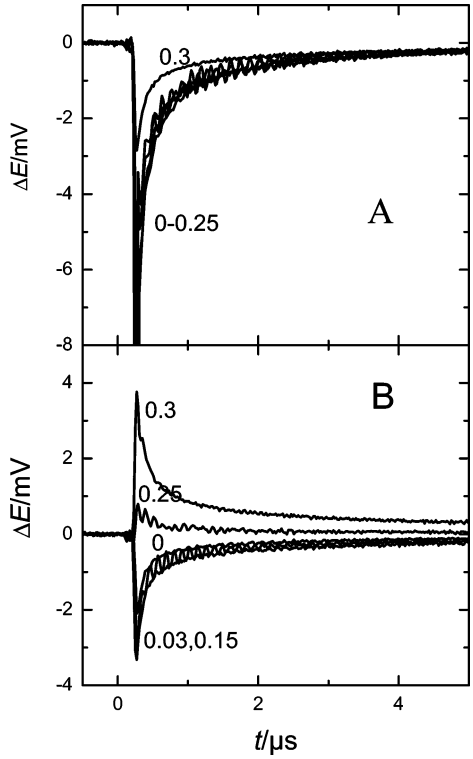

Figure 7. Comparison of the laser-induced potential transients obtained with several Bi coverages, as labeled in the figure, at (A) 0.15 V and (B) 0.45 V in 0.1 M $KClO_4$ + 1 mM $HClO_4$.

As a test to see if the potential relaxation is following the decrease of the temperature after the laser pulse, the same potential transients of Figure 6 have been plotted as function of $1/\sqrt{t}$ in Figure 8. According to eq 14, this should give straight lines, whose slopes are proportional to the thermal coefficient of the double layer, $(\partial\Delta_S^M\phi/\partial T)_q$. For the sake of clarity, the lower and higher potential regions have been separated into two different plots. In the lower potential region, between 0.15 and 0.5 V, the plots are nearly linear, indicating that the kinetic complications due to hydrogen adsorption are small under these conditions. On the other hand, a clear nonlinear response is obtained in the higher potential region. This region coincides with the process of the oxidation/reduction of bismuth, and the nonlinearity is reflecting the slow response of this process to the temperature perturbation, involving the formation and disappearance of oxygenates species.

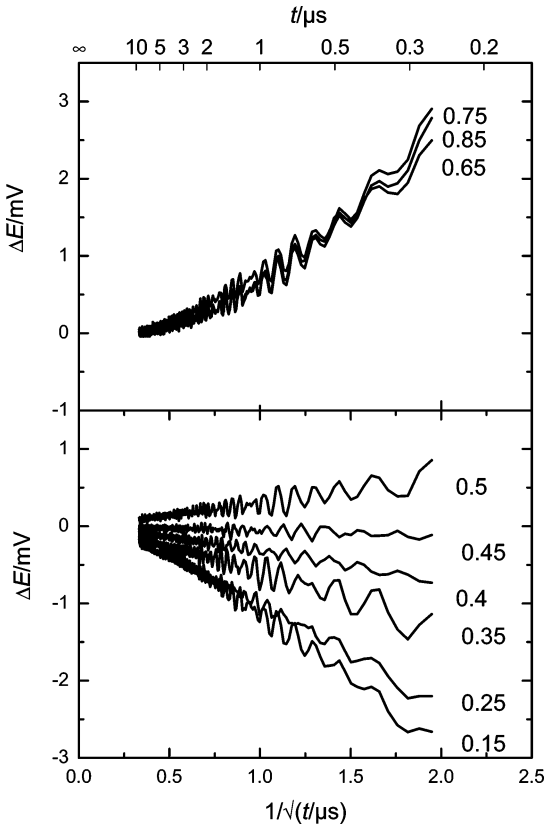

Figure 8. Laser-induced potential transients shown in Figure 6, plotted as a function of $1/\sqrt{t}$. The curves have been separated in two graphs for the sake of clarity.

4. Discussion

Within the above framework, in the absence of kinetic complications, the main contribution to the laser-induced potential transients comes from the thermal coefficient of the potential drop across the double layer, $(\partial\Delta_S^M\phi/\partial T)_q$. According to this, the different magnitude and sign of the potential transients is mainly reflecting the variation of this parameter with the electrode potential. According to the traditional models of the electrochemical double layer, the overall potential drop at the interface can be split into two contributions, due to the diffuse and the inner layers. It is also usually assumed that the potential drop in the diffuse layer follows the Gouy−Chapman theory for sufficiently diluted solutions. More recently, it was pointed out that what has been usually considered the inner layer contribution is more precisely described as composed of two contributions, due to the excess polarization of the water, ϕ_w, and the electron spillover, χ_e[59]

$$\Delta_S^M\phi = \phi_2 + \phi_w + \chi_e \tag{15}$$

Consequently, the thermal coefficient can be divided into three contributions

$$\left(\frac{\partial\Delta_S^M\phi}{\partial T}\right)_q = \left(\frac{\partial\phi_2}{\partial T}\right)_q + \left(\frac{\partial\phi_w}{\partial T}\right)_q + \left(\frac{\partial\chi_e}{\partial T}\right)_q \tag{16}$$

The first term, $(\partial\phi_2/\partial T)_q$, can be calculated from the Gouy-Champman equation and represents only a small contribution in concentrate electrolyte solutions.[47] The last term is also usually considered small.[59] Therefore, the overall coefficient $(\partial\Delta_S^M\phi/\partial T)_q$ is mainly determined from the change in the polarization of solvent molecules. Therefore, the sign of the

potential transients can be considered an indication of the sign of the dipolar contributions to the overall potential drop due to the water orientation. At low potentials, the solvent dipoles are expected to be oriented with the positive end toward the metal, giving a positive contribution to the overall potential drop. The effect of the rise of the temperature is a decrease of this positive contribution, resulting in the observed negative potential transient. At higher potentials, the increase of the temperature induces a decrease in a negative dipolar contribution, resulting in a positive transient. The potential of zero transient (pzt) coincides with the potential where the average dipolar contribution is zero.

The same discussion can be done in terms of the entropy of formation of the double layer. It can be shown that the thermal coefficient is related to the entropy of formation of the double layer by the following expression:[47,49]

$$\left(\frac{\partial \Delta_s^M \phi}{\partial T}\right)_q = -\left(\frac{\partial \Delta S}{\partial q}\right)_T \qquad (17)$$

ΔS is defined as the difference in the entropy of the constituents of the interphase when they are forming it and when they are present in the bulk of the adjoining phases.[49] According to eq 14, at the pzt, $(\partial \Delta_S^M \phi/\partial T)_q = (\partial \Delta S/\partial q)_T = 0$. This implies that the curve ΔS vs q has an extremum at this potential. This extremum will be a maximum if the transient changes from negative to positive when the potential is increased above the pzt. In consequence, the pzt can be identified with the pme of double-layer formation. According to the classical models of the electrified interphase, the maximum entropy is achieved when there is a maximum disorientation in the layer of water molecules next to the electrode surface. This state is expected to be achieved at a potential close to the pzc, because when the electrode surface is charged, the water dipole tends to orient according to the electric field. This vision agrees well with the condition of zero dipolar contribution at the pzt, stated above. The pme has been measured for mercury[47,49] and gold electrodes,[44,50] and it is located at slightly negative polarization with respect to the pzc. This observation has been explained by considering that there is a specific interaction between the water molecules and the metal surface that tends to naturally orient the dipoles with the oxygen toward the metal. Then, at the pzc, there is a positive thermal coefficient, and a small excess of negative charge is necessary to compensate this natural orientation.

From the previous discussion, we can conclude that one significant parameter that can be obtained from the laser-induced potential transients is the value of the potential where the transient is zero, since this potential can be identified with the pme. These potential values have been plotted as a function of the bismuth coverage in Figure 9 for the two studied solutions. The potential values have been converted to the SHE scale to facilitate the comparison. The general trend is the same for the two solutions: the pzt is first shifted to positive potentials as the bismuth coverage increases up to ca. $\theta_{Bi} = 0.15$. For higher bismuth coverages, the pzt sharply decreases to negative potentials. The values obtained at pH = 1 are equal, within the experimental error, to those obtained at pH = 3, except in the range of intermediate bismuth coverages, where more positive potential values of the pzt are obtained at the former pH.

Bismuth adlayers have been characterized in UHV by Auger electron spectroscopy, thermal desorption mass spectrometry, low-energy electron diffraction (LEED), and work function measurements.[51] This study revealed that bismuth adsorption

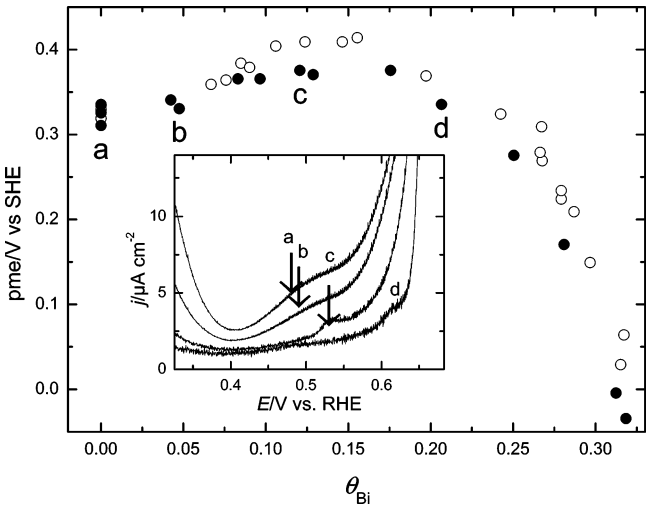

Figure 9. Plot of the potential of zero transient (pzt), identified with the potential of maximum entropy (pme), as a function of bismuth coverage, measured in (a) 0.1 M $HClO_4$ (open circles); (b) 0.1 M $KClO_4$ + 1 mM $HClO_4$ (closed circles). Inset: zoom in the voltammetric profile in 0.1 M $KClO_4$ + 1 mM $HClO_4$ for several Bi coverages. The pzt is marked with an arrow, and the labels a to d indicate the corresponding points in the main plot.

causes a marked decrease of the work function with a saturation value for the work function change of ca. −2.0 eV. This observation implies some ionic character for the Bi−Pt bond, with the bismuth adatoms being partially positively charged. This decrease of the work function is expected to be translated into a displacement to negative potentials of the pzc, in the electrochemical environment, following the proposed parallelism between work function and pzc.[52] Consequently, the displacement to negative potentials of the pzt observed for $\theta_{Bi} > 0.15$ is likely reflecting this shift of the pzc. In other words, the existence of positively charged bismuth adatoms will induce the orientation of the water molecules with the oxygen toward the surface, resulting in a negative dipolar contribution, ϕ_w, and a positive thermal coefficient. This is the trend exemplified in Figure 7B, where the increase of bismuth coverage finally changes the sign of the laser-induced potential transient at 0.45 V.

More difficult to interpret is the initial positive shift of the pzt for low bismuth coverage ($\theta_{Bi} < 0.15$), since this goes against the expected shift of the pzc. It has been shown that in UHV conditions bismuth forms several hexagonal ordered structures on a Pt(111) surface, depending on the coverage, namely, a $p(2 \times 2)$, $(\sqrt{3} \times \sqrt{3})R30°$, $p(3 \times 3)$, and $p(4 \times 4)$. The coverages corresponding to these structures agree well with the Auger data: 0.25, 0.33, 0.44, and 0.56, respectively. The $(\sqrt{3} \times \sqrt{3})R30°$ superstructure was also found in bismuth adlayers formed in an electrochemical environment and subsequently transferred to UHV.[28] Coverages higher than 0.33 have also been achieved in an electrochemical environment, but they lead to a complex redox behavior, with the peak at 0.67 V splitting into multiple peaks.[27,28] Also, this exceeding Bi appears to be less strongly attached to the surface and has been avoided in the present study. It is tempting to say that the change in the trend observed in the plot of Figure 9 is due to the completion of an ordered structure with $\theta_{Bi} = 0.25$. However, this does not seem to be a satisfactory explanation for the following reasons. First, the change in the trend is located at significantly lower coverages. Also, the work function exhibits a monotonic decrease up to the saturation coverage that is expected to be reflected in a monotonic decrease of the pzc. Moreover,

preliminary work with other adatoms shows a similar behavior for the pzt at low coverages, suggesting that the slight displacement to positive potentials of the pzt at low coverage is caused by a more general phenomenon.[60]

The trend observed at low coverages can be described by stating that water molecules tend to stay with the hydrogen toward the metal at higher potentials, while at the same potentials, they have already turned down if bismuth is not present. One tentative explanation for this behavior can be proposed, considering the effect of bismuth adatoms on adjacent platinum atoms. We can expect that bismuth polarizes the platinum, making it more negative, while it becomes positive itself. This increases the range of potentials where the water dipoles are oriented with the positive end (hydrogen) toward the platinum surface. This would imply that there are two contributions: the positive bismuth adatoms tend to orient the water with the oxygen toward the metal, while the negative platinum tends to orient the dipoles in the opposite direction. For low coverages, the effect caused by the free platinum areas would predominate. For high coverages, the uncovered platinum areas are less predominant, while the surface as a whole becomes more positive due to the decrease of the overall pzc. Interestingly, a positive shift of the work function has been observed when water is dosed on a precovered potassium surface, indicating that water is coadsorbed with the alkali cation with the positive end of the dipole toward the metal.[61] One objection can be raised against this hypothesis: as stated before, preliminary results with other adatoms indicate a similar trend in the low-coverage region regardless of the electronegativity of the adatom, suggesting that the increase of the pzt at low coverage is not related with the ionic character of the bismuth−platinum bond.[60]

A second phenomenon that can be invoked to explain the trend observed at low coverages is the disrupting effect of adatoms on the possible formation of extended water networks. This would be equivalent to a third-body effect and would not depend on the electronegativity of the adatom. In the absence of surface modifiers, the optimization of hydrogen bonding is a key factor determining the structure of water adlayers, usually leading to clustering and formation of extended water networks.[62] The net orientation of the water clusters results from the balance between electrostatic and hydrogen bonding interactions. It is expected that the collaborative effect from hydrogen bonding would lead to a net orientation of the water dipoles with the oxygen toward the metal, leaving the hydrogen atoms toward the solution. The destabilization of this structure after the adatom adsorption would facilitate the turnover of the water dipoles to the hydrogen-toward-the-metal orientation, that would take place at a less negative potential, i.e., shifting the pzt toward positive potentials. Implicit in this argument is the fact that the pme is expected to be located at potentials lower that the pzc, since at the pzc, there would be a natural orientation of the water network with the oxygen toward the metal, resulting either from a chemical interaction between the lone pair of electrons on the oxygen and the empty orbitals of the metal or from the optimization of the hydrogen bonding on the water network. The position of the pzc on Pt(111) in perchloric acid solution is not known, since it cannot be directly measured. However, indirect estimation of the pzc from CO charge displacement studies tend to locate it at potentials lower that the pme value determined from the laser-induced temperature jump measurements. This is in contradiction to the previous arguments, although consideration of several corrections to the previous estimation could lead to a reconciliation of both measurements.[63] Clearly, more work is needed to fully understand these aspects of the electrochemistry of Pt(111) single-crystal electrodes. Finally, it is worth pointing out that the pzt of Bi-free Pt(111) coincides with the capacitance peak observed in the double-layer region in 0.1 M $KClO_4$ + 1 mM $HClO_4$.[45] It is remarkable that this coincidence is maintained when the surface is modified by Bi adsorption at low coverage (inset Figure 9). In this way, the positive shift of the pzt parallels that of the capacitive hump.

We want to emphasize that the previous discussion is based on several simplifications, like the consideration of thermodiffusion potential, diffuse layer, and electron spillover contribution as second-order contributions to the overall potential transient. Other factors that also need consideration are as follows: (i) mobility of bismuth adatoms and its influence on the entropy of formation of the double layer and, also, how this mobility changes with the electrode potential (in this respect, it is reasonable to assume that mobility of bismuth adatoms will be much slower than reorganization phenomena on the solvent, and this will also be a minor contribution); (ii) influence of the bismuth adatoms on the spillover of electrons and their entropic contribution. Detailed calculations are needed to fully understand the importance of electronic contributions to the thermal coefficient of the double layer, and this falls beyond the purpose of the present paper.

5. Conclusions

The laser-induced temperature jump method has been applied to study the effect of bismuth adatoms on the properties of the double-layer region formed between a Pt(111) electrode and perchloric acid solutions. The sign of the laser-induced potential transients is considered an indication of polarity of the dipolar contribution to the potential drop at the interface. Therefore, the important parameter deduced from this study is the potential where this dipolar contribution changes its sign. This pzt can be identified with the pme of formation of the double layer. The variation of the pme with the bismuth coverage shows that at high coverages a marked decrease of the pme is observed, mimicking the expected behavior of the pzc. However, at low coverages, the pme slightly increases when the surface is modified with a small amount of bismuth. From the different hypotheses given to explain this increase, the possible disruption of hydrogen-bonded water networks seem to be the most plausible, although still some questions remain open that call for more work to fully understand the observed phenomena. Theoretical calculations are especially needed to account for the effect of electronic interaction on the dependence of the interfacial potential drop on the temperature.

Acknowledgment. Financial support from the MCyT (Spain) through project BQU2003-04029 is gratefully acknowledged. N.G. thanks the MEC (Spain) for the award of a FPU grant. V.C. acknowledges financial support from the MEC under the Ramon y Cajal program. We express our gratitude for the help and useful discussions with F. Gallud and Dr. C. Antón in the development of the electronic instrumentation.

References and Notes

(1) Clavilier, J.; Fernández-Vega, A.; Feliu, J. M.; Aldaz, A. *J. Electroanal. Chem.* **1989**, *258*, 89.
(2) Fernández-Vega, A.; Feliu, J. M.; Aldaz, A.; Clavilier, J. *J. Electroanal. Chem.* **1989**, *258*, 101.
(3) Clavilier, J.; Fernández-Vega, A.; Feliu, J. M.; Aldaz, A. *J. Electroanal. Chem.* **1989**, *261*, 113.
(4) Fernández-Vega, A.; Feliu, J. M.; Aldaz, A.; Clavilier, J. *J. Electroanal. Chem.* **1991**, *305*, 229.
(5) Chang, S.-C.; Ho, Y.; Weaver, M. J. *Surf. Sci.* **1992**, *265*, 81.

(6) Herrero, E.; Fernández-Vega, A.; Feliu, J. M.; Aldaz, A. *J. Electroanal. Chem.* **1993**, *350*, 73−88.
(7) Llorca, M. J.; Feliu, J. M.; Aldaz, A.; Clavilier, J. *J. Electroanal. Chem.* **1994**, *376*, 151−160.
(8) Herrero, E.; Feliu, J. M.; Aldaz, A. *J. Electroanal. Chem.* **1994**, *368*, 101−108.
(9) Llorca, M. J.; Herrero, E.; Feliu, J. M.; Aldaz, A. *J. Electroanal. Chem.* **1994**, *373*, 217−225.
(10) Kizhakevariam, N.; Weaver, M. J. *Surf. Sci.* **1994**, *310*, 183−197.
(11) Herrero, E.; Llorca, M. J.; Feliu, J. M.; Aldaz, A. *J. Electroanal. Chem.* **1995**, *383*, 145−154.
(12) Herrero, E.; Llorca, M. J.; Feliu, J. M.; Aldaz, A. *J. Electroanal. Chem.* **1995**, *394*, 161−167.
(13) Leiva, E.; Iwasita, T.; Herrero, E.; Feliu, J. M. *Langmuir* **1997**, *13*, 6287−6293.
(14) Climent, V.; Herrero, E.; Feliu, J. M. *Electrochim. Acta* **1998**, *44*, 1403−1414.
(15) Mo, Y. B.; Scherson, D. A. *J. Electrochem. Soc.* **2003**, *150*, E39−E46.
(16) Gomez, R.; Fernandez-Vega, A.; Feliu, J. M.; Aldaz, A. *J. Phys. Chem.* **1993**, *97*, 4769−4776.
(17) Conway, B. E.; Barber, J. H.; Gao, L.; Qian, S. Y. *J. Alloys Compd.* **1997**, *253*, 475−480.
(18) Gómez, R.; Feliu, J. M.; Aldaz, A. *Electrochim. Acta* **1997**, *42*, 1675−1683.
(19) Clavilier, J.; Feliu, J. M.; Aldaz, A. *J. Electroanal. Chem.* **1988**, *243*, 419.
(20) Clavilier, J.; Feliu, J.; Fernández-Vega, A.; Aldaz, A. *J. Electroanal. Chem.* **1989**, *269*, 175−189.
(21) Feliu, J. M.; Fernández-Vega, A.; Aldaz, A.; Clavilier, J. *J. Electroanal. Chem.* **1988**, *256*, 149.
(22) Clavilier, J.; Feliu, J. M.; Fernandez-Vega, A.; Aldaz, A. *J. Electroanal. Chem.* **1990**, *294*, 193−208.
(23) Gómez, R.; Llorca, M. J.; Feliu, J. M.; Aldaz, A. *J. Electroanal. Chem.* **1992**, *340*, 349−355.
(24) Feliu, J. M.; Gómez, R.; Llorca, M. J.; Aldaz, A. *Surf. Sci.* **1993**, *289*, 152−162.
(25) Feliu, J. M.; Gómez, R.; Llorca, M. J.; Aldaz, A. *Surf. Sci.* **1993**, *297*, 209−222.
(26) Dollard, L.; Evans, R. W.; Attard, G. A. *J. Electroanal. Chem.* **1993**, *345*, 205−221.
(27) Evans, R. W.; Attard, G. A. *J. Electroanal. Chem.* **1993**, *345*, 337−350.
(28) Hamm, U. W.; Kramer, D.; Zhai, R. S.; Kolb, D. M. *Electrochim. Acta* **1998**, *43*, 2969−2978.
(29) Smith, S. P. E.; Abruña, H. D. *J. Phys. Chem. B* **1998**, *102*, 3506−3511.
(30) Schmidt, T. J.; Grgur, B. N.; Behm, R. J.; Markovic, N. M.; Ross, P. N. *Phys. Chem. Chem. Phys.* **2000**, *2*, 4379−4386.
(31) Climent, V.; Herrero, E.; Feliu, J. M. *Electrochem. Commun.* **2001**, *3*, 590−594.
(32) Schmidt, T. J.; Stamenkovic, V.; Attard, G. A.; Markovic, N. M.; Ross, P. N. *Langmuir* **2001**, *17*, 7613−7619.
(33) Schmidt, T. J.; Stamenkovic, V. R.; Lucas, C. A.; Markovic, N. M.; Ross, P. N. *Phys. Chem. Chem. Phys.* **2001**, *3*, 3879−3890.
(34) Ball, M.; Lucas, C. A.; Markovic, N. M.; Murphy, B. M.; Steadman, P.; Schmidt, T. J.; Stamenkovic, V.; Ross, P. N. *Langmuir* **2001**, *17*, 5943−5946.
(35) Blais, S.; Jerkiewicz, G.; Herrero, E.; Feliu, J. M. *J. Electroanal. Chem.* **2002**, *519*, 111−122.
(36) Herrero, E.; Feliu, J. M.; Aldaz, A. *J. Catal.* **1995**, *152*, 264−274.
(37) Feliu, J. M.; Fernandez-Vega, A.; Orts, J. M.; Aldaz, A. *J. Chim. Phys. Phys.-Chim. Biol.* **1991**, *88*, 1493−518.
(38) Schmidt, T. J.; Behm, R. J.; Grgur, B. N.; Markovic, N. M.; Ross, P. N. *Langmuir* **2000**, *16*, 8159−8166.
(39) Macia, M. D.; Herrero, E.; Feliu, J. M. *J. Electroanal. Chem.* **2003**, *554*, 25−34.
(40) Orts, J. M.; Rodes, A.; Feliu, J. M. *J. Electroanal. Chem.* **1997**, *434*, 121−127.
(41) Rhee, C. K.; Kim, D.-K. *J. Electroanal. Chem.* **2001**, *506*, 149−154.
(42) Zhou, W. P.; Kibler, L. A.; Kolb, D. M. *Electrochim. Acta* **2004**, *49*, 5007−5012.
(43) Zhou, W. P.; Kibler, L. A.; Kolb, D. M. *Electrochim. Acta* **2002**, *47*, 4501−4510.
(44) Climent, V.; Coles, B. A.; Compton, R. G. *J. Phys. Chem. B* **2002**, *106*, 5258−5265.
(45) Climent, V.; Coles, B. A.; Compton, R. G. *J. Phys. Chem. B* **2002**, *106*, 5988−5996.
(46) Climent, V.; Coles, B. A.; Compton, R. G.; Feliu, J. M. *J. Electroanal. Chem.* **2004**, *561*, 157−165.
(47) Benderskii, V. A.; Velichko, G. I. *J. Electroanal. Chem.* **1982**, *140*, 1−22.
(48) Smalley, J. F.; Krishnan, C. V.; Goldman, M.; Feldberg, S. W.; Ruzic, I. *J. Electroanal. Chem.* **1988**, *248*, 255−82.
(49) Harrison, J. A.; Randles, J. E. B.; Schiffrin, D. J. *J. Electroanal. Chem.* **1973**, *48*, 359−381.
(50) Silva, F.; Sottomayor, M. J.; Hamelin, A. *J. Electroanal. Chem.* **1990**, *294*, 239−251.
(51) Paffett, M. T.; Campbell, C. T.; Taylor, T. N. *J. Chem. Phys.* **1986**, *85*, 6176−6185.
(52) Trasatti S. In *Comprehensive Treatise of Electrochemistry*; Bockris, J. O., Conway, B. E., Yeager, E., Eds.; Plenum: New York, 1980; Vol. 2, pp 45−81.
(53) Clavilier, J.; Armand, D.; Sun, S.-G.; Petit, M. *J. Electroanal. Chem.* **1986**, *205*, 267−277.
(54) Agar J. N. In *Advances in Electrochemistry and Electrochemical Engineering*; Delahay, P., Tobias, C. W., Eds.; Wiley-Interscience: New York, 1963; Vol. 2, pp 31−121.
(55) Climent V.; Gómez, R.; Orts, J. M.; Aldaz, A.; Feliu, J. M. In *The Electrochemical Society Proceedings* (Electrochemical Double Layer); Korzeniewski, C., Conway, B. E., Eds.; The Electrochemical Society, Inc.: Pennington, NJ, 1997; pp 222−237.
(56) Von Allmen, M.; Blatter, A. *Laser-beam interactions with materials: physical principles and* applications, 2nd updated/ed.; Springer: Berlin, 1995; xi, 194.
(57) Holman, J. P. *Heat Transfer*, 9th ed.; McGraw-Hill Science: Blacklick, Ohio, 2001.
(58) *Handbook of optical constants of solids;* Academic Press Handbook Series; Palik, E. D., Ed.; Academic Press: London, 1985.
(59) Guidelli, R.; Aloisi, G.; Leiva, E.; Schmickler, W. *J. Phys. Chem. B* **1988**, *92*, 6671−6675.
(60) Garcia-Araez, N.; Climent, V.; Feliu, J. M. 57th Annual Meeting of the International Society of Electrochemistry, Book of Abstracts, S8-0-5, August 27−September 1, 2006, Edinburgh.
(61) Bonzel, H. P.; Pirug, G.; Muller, J. E. *Phys. Rev. Lett.* **1987**, *58*, 2138−2141.
(62) Henderson, M. A. *Surf. Sci. Rep.* **2002**, *46*, 1−308.
(63) Climent, V.; Garcia-Araez, N.; Herrero, E.; Feliu, J. M. *Russ. J. Electrochem.* **2006**, *42*, 1145−1160.